Conference Proceedings

EuroSun 2014
Aix-les-Bains (France), 16 – 19 September 2014

Characterization Of A Medium Temperature Concentrator For Process Heat – Tracking Error Estimation

Fabienne Sallaberry[1,2,*], Fabrizio Alberti[3], Jose-Luis Torres[2], Luigi Crema[3], Mattia Roccabruna[3] and Ramon Pujol-Nadal[4]

[1] CENER (National Renewable Energy Center, Sarriguren-Pamplona (Spain), email: fsallaberry@cener.com[2] UPNA (Public University of Navarra), Pamplona (Spain)

[3] FBK (Fondazione Bruno Kessler), Povo-Trento (Italy)

[4] University of Balearic Islands, Physics Department. Palma de Mallorca (Spain)

Abstract

Concentrating solar collectors could be used in industry to meet heating demands. In this study, a solar thermal concentrator is investigated. This system was designed and built within a European project, DIGESPO, and a prototype has been installed on a pharmaceutical plant for process heat generation in Malta. In this paper, the optical efficiency of this collector was characterized using the input and output measured data obtained during a testing campaign lasting than two months. A thermal analysis was undertaken to estimate how the solar tracker precision of this collector could influence the solar collector optical efficiency, based on tracker installation error estimation and the transverse incidence angle modifier curve determined by ray-tracing program. The results obtained were a optical efficiency η_0 of 30.9% and a maximum optical lost due to incidence angle of 0.5%.

Keywords: Collector testing; variable geometry; optical and thermal characterization; solar tracking error; process heat

1. Introduction

The solar tracking systems are used to orient the solar concentrator with the sun direction in order to concentrate the direct solar radiation onto a unique focus point or line. A receiver is located on the focus line of the linear collector through which a thermal fluid is circulated. In this way the receiver transforms the solar radiation into heat by increasing the heat transfer fluid temperature.

In order to have an efficient solar concentration, the tracking system has to be appropriately integrated with the optics of the solar system since if the concentration ratio is high but the required tracking steps or collocation is not perfectly set, the efficiency of the solar collector may be compromised.

A small size concentrated solar collector has been installed in the industrial area of Birzebbuga in the Island of Malta, after being designed and realized as part of the European funded project called DIGESPO. The developed system integrates small-scale concentrator optics with moving and tracking components, solar absorbers in the form of evacuated tube collectors, a heat transfer fluid, a Stirling engine with generator, and ancillary heating and/or cooling systems.

In this particular collector the receiver tubes are fixed, and the reflector is moving in order to track the sun. Hence the relative position between the reflectors and receiver is not constant during the day. This collector can be defined as a peculiar variable geometry collector. In this paper, the characterization of the optical and thermal behavior of this prototype was measured over a two months testing period. The ISO 9806 (2013) was

© 2015. The Authors. Published by International Solar Energy Society
Selection and/or peer review under responsibility of EuroSun2014 Scientific Committee
doi:10.18086/eurosun.2014.01.07 Available at http://proceedings.ises.org

used as a baseline standard for the data treatment and to calculate the characteristic parameters of this collector. Finally a sensitivity analysis was performed to estimate the tracking error, which leads to a conversion efficiency or optical efficiency on the collector production.

2. Materials

2.1 Solar Concentrator

The system is composed of 4 modules with 4 tubes each, for a total collecting area of approximately 12 m^2. A single collector is 2000 mm long, 400 mm wide and 200 mcm of focal length, with a concentration ratio C = 10.6 (See Fig. 1). The evacuated solar tubes are 12 mm in diameter prepared with a selective coating absorber, and are located on the focus lines. The reflector is a very thin flexible glass mirror (< 1 mm) developed during the DIGESPO project. The overall mirror reflectivity was verified at 0.954. See references (Alberti et al. 2012a, 2013; Crema, 2013) for more information.

Fig. 1: Picture of the DIGESPO solar collector

The absorber consistes of four thin coatings, namely two layers of a ceramic and metallic composite material plus an anti-reflection and IR reflecting layer on top and back respectively,. The up-scaled receiver tube with a Cer.Met. coating based on TiO2–Nb, obtained an absorptance α of 0.94 and emittance ε of 0.1 (at 350°C). A second Cer.Met. coating of SiO2–W demonstrated an absorptance α of 0.93 and emittance ε of 0.09 (at 350°C). A full-evacuated solar tube has been designed and manufactured, with absorber of 12 mm in diameter and 2 meters long. See the references for more information (Alberti et al. 2012b).

2.2 Testing bench

The inputs and outputs of the collector were monitored, using various sensors connected to a data logger. The main inputs and outputs were the inlet and outlet temperatures of the thermal fluid through the collector, the mass flow rate and the direct normal solar irradiance. Two pyranometers were used for the global and diffuse solar irradiance measurements and were mounted on one of the collectors. For the diffuse irradiance measurement a pyranometer with a shadow ring was used.

3. Theory and calculation

3.1. Thermal performance

The model for the collector's efficiency can be written as described in Eq. 1, according to ISO 9806 (2013) standard and assume no diffuse solar irradiance dependency for the concentrator:

$$\frac{Q}{A_a} = \eta_0 K_b(\theta_T, \theta_L) G_{bT} - c_1(t_m - t_a) - c_2(t_m - t_a)^2 - c_5 \, dt_m / dt \qquad \text{(eq. 1)}$$

The first term η_0 represents the conversion efficiency or optical efficiency which is the product $F'(\rho\gamma\tau\alpha)_{en}$ (where F' the thermal efficiency, ρ the reflector reflectance, γ the intercept factor, τ the cover transmittance and α the absorber absortance); the second and third terms, c_1 and c_2, represent the thermal losses; and the

fourth term, c_5,represents the thermal capacity of the collector. The aperture area was measured from the reflectors pieces as 14.104 m^2. G_{bT} is the direct solar irradiance on the collector plane (direct normal solar irradiance (DNI)*cos(θ)), t_m is the average fluid temperature in the collector and t_a is the ambient temperature. K_b is the incidence angle modifier to direct solar radiation, θ_T and θ_L are the transversal and longitudinal angles respectively.

3.2. Optical simulation

The ray-tracing software used in order to simulate the optical efficiency dependency of the collector to the incidence angle, which is called incidence angle modifier IAM, K_b, was done using a Fortran program for different transversal and longitudinal angles (θ_T and θ_L respectively). This software was explained in Pujol et al. (2012) and validated experimentally in Sallaberry et al. (2014). In this program four kinds of surfaces has been introduced: specular surfaces, opaque surfaces, interface surfaces (to implement glasses), and absorber surfaces (the receiver). The program calculates ray trajectories from one source (called the sun window) which emits to all the surfaces of the system.

In the ray-tracing, the geometry of the solar concentrator is described by a parabolic reflector with focal length of 200 mm and a cylindrical tube located in that focal line. The ray trajectories from the sun window are simulated over each surface of the collector. The simulation optical efficiency η_0 is calculated dividing the number of photons reaching the absorber surface with the number of photon from the aperture area.

Table 1 shows the geometry and the physical properties introduced as inputs in the ray-tracing program. The simulation was repeated for different transverse incidence angles on the collector ($\theta_T \in [0, 10]^o$) along the tracking plane with steps of 0.1°.

Table. 1. Optical properties of the collector

Element (dimensions or optical properties)	Value	Unity
Reflector parabola length	2000	mm
Reflector parabola width	400	mm
Focal length	200	mm
Mirror solar reflectance ρ	0.95	-
Glass tube length	2000	mm
Receiver glass tube outer diameter	55,7	mm
Glass tube thickness	1	mm
Glass tube transmittance τ	0.954	-
External diameter of the receiver	12	mm
Absorber solar absortance α	0.94	-

The result of this simulation identified the profile of the incidence angle modifier on the transversal plane of the collector for different longitudinal incidence angle, $K_b(\theta_T)$.

The collector's parameters and the incidence angle modifier characterised by ray-tracing are both used to estimate the optical efficiency losses ($\Delta\eta$) and the angular tracking error in the transversal plane ($\theta_{track} = \theta_T$) (See Fig. 2).

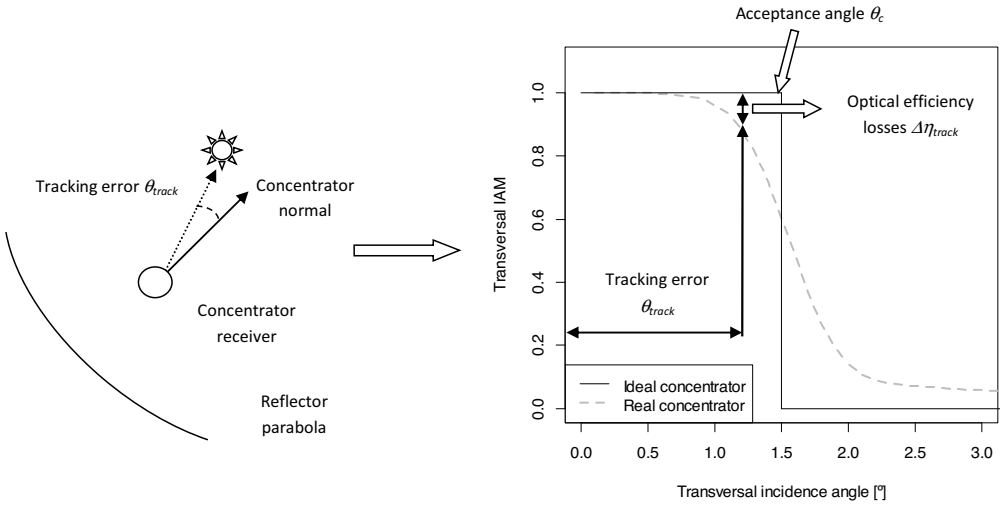

Figure 2: Scheme of the tracking error analysis

3.3. Sensibility analysis of installation on the tracking error

The second objective of this study was the estimation of incidence angle on the transversal plane of the collector in order to have the optimum tracking angle movement algorithm. Considering the longitudinal and transversal incidence angles as the projection of the sun vector on the two planes (the longitudinal plane parallel to the receiver tubes and the transversal plane in the parabolic plane perpendicular to the tubes), the sun vector will be defined as the coordinates of the solar vector in the first reference (X_0, Y_0, Z_0).

The two angles, α_s the solar elevation and γ_s the solar azimuth, were determined using the algorithm by Blanco-Muriel et al. (2001). Three referential rotations were necessary in order to obtain the sun vector in the collector referential and to calculate the incidence angles, as shown in Fig. 3. The first reference rotation is around the Z axis with respect to the collector azimuth γ_C angle; the second rotation is around the Y axis with the collector tilt β_C angle; the third rotation is around the X axis with the tracking angle α_C.

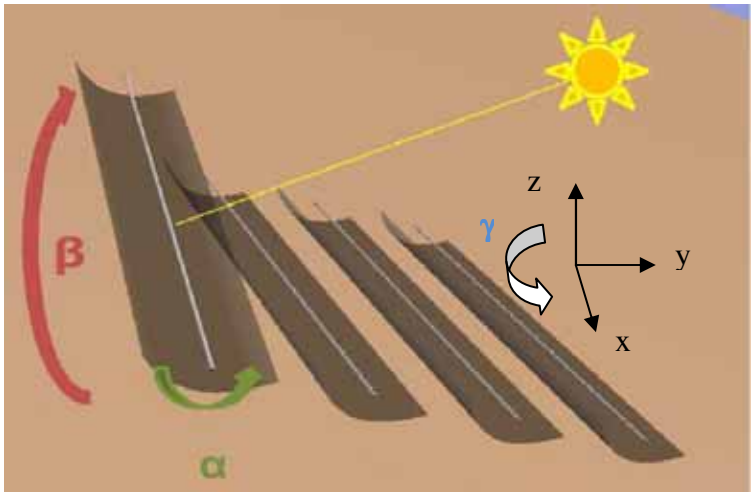

Figure 3: Collector position, orientation and tilt

The reference change is according to the Eq. 2 (See Pujol-Nadal 2014).

$$\begin{pmatrix} X_{rot} \\ Y_{rot} \\ Z_{rot} \end{pmatrix} = \begin{pmatrix} X_0 \\ Y_0 \\ Z_0 \end{pmatrix} \bullet \begin{pmatrix} \cos\gamma_C & \sin\gamma_C & 0 \\ -\sin\gamma_C & \cos\gamma_C & 0 \\ 0 & 0 & 1 \end{pmatrix} \bullet \begin{pmatrix} \cos\beta_C & 0 & \sin\beta_C \\ 0 & 1 & 0 \\ -\sin\beta_C & 0 & \cos\beta_C \end{pmatrix} \bullet \begin{pmatrix} 1 & 0 & 0 \\ 0 & \cos\alpha_C & -\sin\alpha_C \\ 0 & \sin\alpha_C & \cos\alpha_C \end{pmatrix} \quad \text{(eq. 2)}$$

Then, the projections of the solar vector on the longitudinal and transversal planes are defined as the Eq. 3-4.

$\theta_L = \tan^{-1}(X_{rot}/Z_{rot})$ (eq. 3)

$\theta_T = -\tan^{-1}(Y_{rot}/Z_{rot})$ (eq. 4)

If the collector is correctly tracking it means that the projection of the sun vector on the transversal plan is null, which means that $\theta_T = 0$ which is equivalent to Eq. 5:

$$\tan\alpha = -\frac{\cos\alpha_s \cos\gamma_S \sin\gamma_C - \cos\alpha_s \sin\gamma_S \cos\gamma_C}{\cos\alpha_s \cos\gamma_S \cos\gamma_C \sin\beta_C + \cos\alpha_s \sin\gamma_S \sin\gamma_C \sin\beta_C + \sin\alpha_s \cos\beta_C} \quad \text{(eq. 5)}$$

Which leads to the Eq. 6.

$$\alpha = \tan^{-1}\left(\frac{\cos\alpha_s \cos\gamma_s \sin\gamma_C - \cos\alpha_s \sin\gamma_s \cos\gamma_C}{\cos\alpha_s \cos\gamma_s \cos\gamma_C \sin\beta_C + \cos\alpha_s \sin\gamma_s \sin\gamma_C \sin\beta_C + \sin\alpha_s \cos\beta_C}\right) \quad \text{(eq. 6)}$$

For a perfectly south oriented collector the tracking the formula is Eq. 7 which is a reduction of Eq. 6 for $\gamma_C = 0^o$, and which is used in the tracking algorithm for the DIGESPO collector.

$$\alpha = \tan^{-1}\left(\frac{\cos\alpha_s \sin\gamma_s}{\sin\beta_C \cos\alpha_s \cos\gamma_s + \cos\beta_C \sin\alpha_s}\right) \quad \text{(eq. 7)}$$

The Eq. 7 is also similar to the one in the report by Marion and Dobos (2013).

Also, the transverse and longitudinal angles, θ_T and θ_L, have been calculated assuming that the installation of the collector to the south is perfect ($\gamma_C = 0^o$), Eq. 7. However, the Eq.6 is used to estimate the possible deviation on the south in the collector tracker mounting.

The collector tilt β_C was measured on the receiver tube as 34.0° with a precision of $u(\beta_C) = \pm 0.5^o$.

The collector orientation γ_C has been fixed using the shadow of a weight hanged on a cord at solar noon, but this technique could results in some error as it is quite difficult to keep the rope perfectly vertical because of the wind. So, the error to the south orientation was estimated up to $u(\gamma_C) = \pm 1^o$.

The tracking rotation angle step $\Delta\alpha$ is around ±0.036° (10.000 motors step on 360°) additionally with ±0.005° error due to the solar algorithm used by the tracker software, and ±0.008° error due to time setting imprecision of the tracker controller (2 second). The uncertainty of the tracking rotation angle will be $u(\alpha_C) = \sqrt{(0.036)^2 + (0.005)^2 + (0.008)^2} = 0.037^o$.

Other important parameters are the daily stroke of the tracking which is 125° and the "offset east" which is 24.5°.

The optical losses ($\Delta\eta$) were defined by using the transversal IAM fit and the tracker angular error (θ_T), according to Eq. 8:

$$\Delta\eta_{track} = \left(1 - K_b(\theta_T)\right) \cdot 100 \quad \text{(eq. 8)}$$

The optical losses due to the tracking system ($\Delta\eta_{track}$) was calculated by using the transversal IAM fit and all the three rotation angles uncertainties ($u(\alpha_C)$,$u(\beta_C)$,$u(\gamma_C)$).

The optical losses error were estimated using an uncertainty estimation of the transversal incidence angle and calculated by the propagation law of errors (ISO/IEC Guide 98-3, 2008) which define the uncertainty of the parameter $u(y)$ from different variable x_i as the Eq. 9.

$$u(y) = \sqrt{\sum_{i=1}^{N} \left(c_i \cdot u(x_i)\right)^2} \qquad \text{(eq. 9)}$$

So, the uncertainty of the transverse incidence angle would be represented by Eq. 10 considering the three rotation angles parameters.

$$u(\theta_T) = \sqrt{\left(u(\gamma_C) \cdot \frac{\partial \theta_T}{\partial \gamma_C}\right)^2 + \left(u(\beta_C) \cdot \frac{\partial \theta_T}{\partial \beta_C}\right)^2 + \left(u(\alpha_C) \cdot \frac{\partial \theta_T}{\partial \alpha_C}\right)^2} \qquad \text{(eq. 10)}$$

Finally, the uncertainty of the optical losses, u($\Delta\eta_{track}$),would be according to Eq. 11.

$$u(\Delta\eta_{track}) = \sqrt{\left(u(\theta_T) \cdot \frac{\partial \Delta\eta_{track}}{\partial \theta_T}\right)^2 + \left(u(K_b) \cdot \frac{\partial \Delta\eta_{track}}{\partial K_b}\right)^2} \qquad \text{(eq. 11)}$$

As there is no formula for the transversal incidence angle modifier $K_b(\theta_T)$ the derivation was calculated by deriving the simulation curve obtained by ray-tracing according to Eq. 12 and 13.

$$\frac{\partial \Delta\eta_{track}}{\partial \theta_T} = \frac{\partial\left(\left(1 - K_b(\theta_T)\right) \cdot 100\right)}{\partial \theta_T} = -100 \frac{\partial\left(K_b(\theta_T)\right)}{\partial \theta_T} \qquad \text{(eq. 12)}$$

$$\frac{\partial \Delta\eta_{track}}{\partial K_b} = \frac{\partial\left(\left(1 - K_b(\theta_T)\right) \cdot 100\right)}{\partial K_b} = -100 \qquad \text{(eq. 13)}$$

The uncertainty of the simulation for the determination of the IAM curve is ± 0.03

4. Results

4.1. Thermal performance

The entire testing period was held over 34 days (between 13/08/2012 and 03/10/2012). Fig. 4 (a-b) shows the variability of the data, spread over a wide range for each input data representing normal operating conditions of the collector: where diffuse solar irradiance on collector aperture $G_{dT} \in [94, 350]$ W.m^{-2}, global solar irradiance on collector aperture $G_T \in [654, 1020]$ W.m^{-2}, and temperature difference between fluid and ambient t_m-$t_a \in [120, 163]$ ºC. The testing at ambient working temperature ($t_m = t_a \pm 3$K as required by the international standard ISO 9806 (2013)) could not be performed since the collector was working in its normal operation range and the oil could not be cooled.

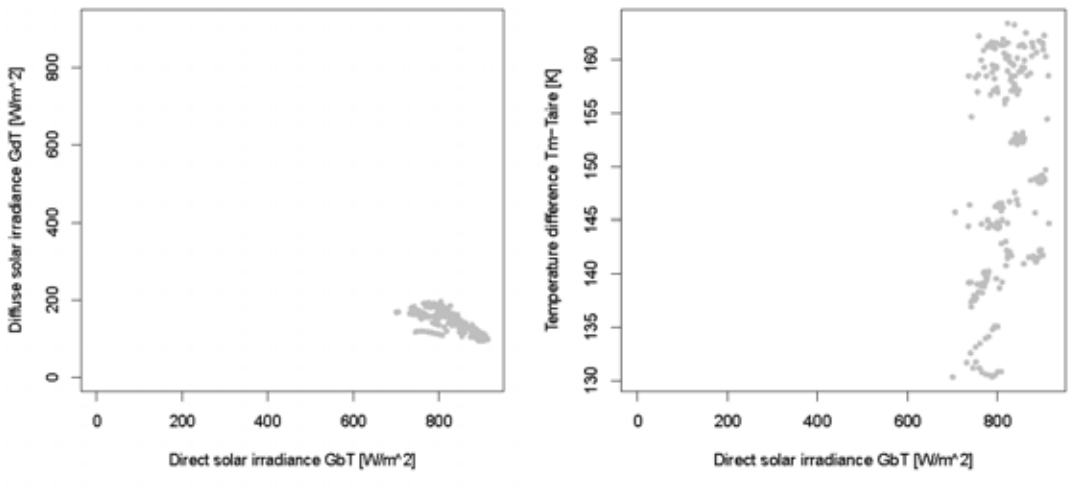

(a) **(b)**

Figure 4: Input data variability (a) diffuse solar irradiance G_{dT} vs direct solar irradiance G_{bT} (b) temperature difference (t_m-t_a) vs direct solar irradiance G_{bT}

The variability of the data is not enough according to ISO 9806 (2013), more particularly the inner temperature which is around the operating temperature range of the collector (only from 148ºC to 189ºC) and complicates the parameter identification according to the model equation Eq 1. Also, the diffuse solar irradiance does not have a lot of variability (~200 W/m^2) due to the fact that the concentrating collector does not work with diffuse radiation.

Table 2 shows the results of the multiple linear regression (MLR) performed for the parameter identification.

Tab. 2: Test results

Parameter	Value and typical uncertainty	Unit
Optical efficiency η_0	0.309 ± 0.046	--
Thermal losses c_1	0.317± 0.253	W.m^{-2}K^{-1}
Thermal capacity c_5	5103 ± 1439	Jm^{-2}K^{-1}

The second heat losses parameter c_2 was ignored due to the high uncertainty. The first heat losses parameter c_1 also showed high uncertainty. Anyway, the poor variability in the mean temperature t_m during the test campaign could not allow a correct characterization of the heat loss parameters. The longitudinal incidence angle modifier was ignored due to its poor variability since the tracking is polar.

The mean error estimation MAE(Q) is 368.16 W and the root mean square error RMSE(Q) is 527.65 W which is 48.3% of the measured power Q values.

Fig. 5 shows the distribution of the instantaneous efficiency values η (between 0.10 and 0.30) versus the reduced temperature difference $(t_m-t_a)/G_{bT}$ (between 0.15 and 0.22) (grey dots) (G_{bT} is the direct solar irradiance on the collector plane (=DNI*cos(θ)), t_m is the average fluid temperature in the collector and t_a is the ambient temperature.). The thermal curve is presented by the black line for a global solar radiation of G_T= 1000 W/m^2. The red brackets present the uncertainty range of the thermal curve. During a conventional low-temperature collector testing the reduced temperature difference obtained was between at least 0 and 0.1 which allows the characterization ofthe heat loss coefficients accurately.

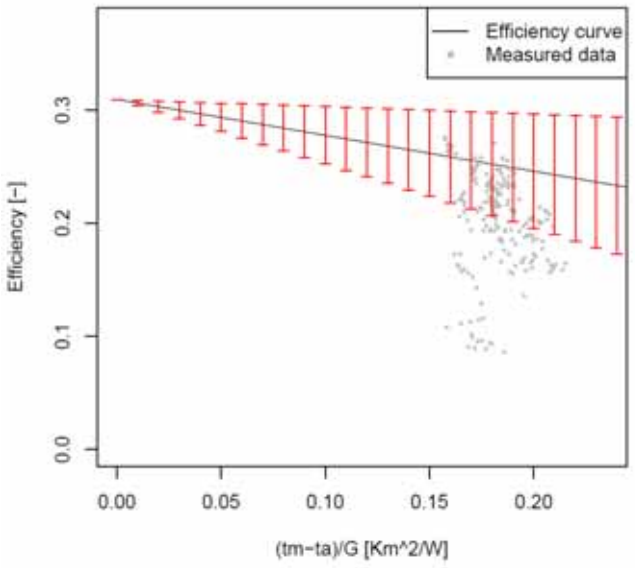

Figure 5 : Efficiency data and curve fitting

The measurement series for output power calculated using model Eq. 1 and the characteristics parameters obtained from Table 2, Q_{mod}, having less than a 10% margin of error with the measured output power, Q_{med}, is 37%. However, the measurement series for the model output power calculated, Q_{mod}, and the measured

output power, Q_{med}, are close for less than 95% the measurement uncertainty

The efficiency at the same temperature also changed during the testing phase, which leads to difficulties in identifying the optical efficiency value, $\eta_0 = F(\rho\gamma\tau\alpha)_{en}$, against the same inner temperature. This could have been due to other thermal losses from the testing bench and degradation of the solar collectors or shadows projected by each parabola over the others thus reducing the incident solar radiation.

Another possible reason for such low optical efficiency is tracking errors due to incorrect installation of the solar tracker. This effect is studied in part 4.3.

4.2. Optical simulation

In this part, the dependency of the optical efficiency η_0 to the incidence angle along the tracking plane was studied. The IAM for different transverse angles is shown in Fig. 6. The number of rays used was 10^7 in the ray-tracing program.

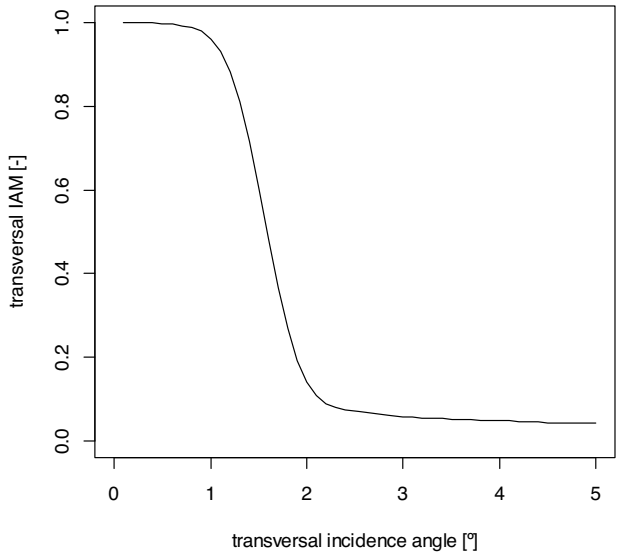

Figure 6: Incidence angle modifier profile

The transversal IAM is close to 1 up to 0.5º. The acceptance angle of the concentrator, which is the angle for an 90% of energy reaching the receiver ($K_b(\theta_T)$>0.90) (Rabl et al. 1980, Zaaiman and Taylor, 2011), found around 1.1º. Then, the transversal IAM drops under 0.5 at 1.6º, and finally is also null from 2º.

4.3. Sensibility of installation on the tracking error

The maximum optical losses ($\Delta\eta$) were calculated by using the transversal IAM curve and the incidence angle (θ_T) from Eq. 8. The uncertainty of the transverse incidence angle according to Eq. 10 was also calculated. Fig. 7 shows the uncertainty transverse incidence angle u(θ_T) ("tetaT" in blue) calculated with its different uncertainty sources u(α_C)$\delta\theta_T/\delta\alpha_C$ (alfa in green), u(β_C)$\delta\theta_T/\delta\beta_C$ (beta in red) and u(γ_C)$\delta\theta_T/\delta\gamma_C$ (gama in black), for one day (21 of June the summer solstice). The uncertainty u(θ_T) is .

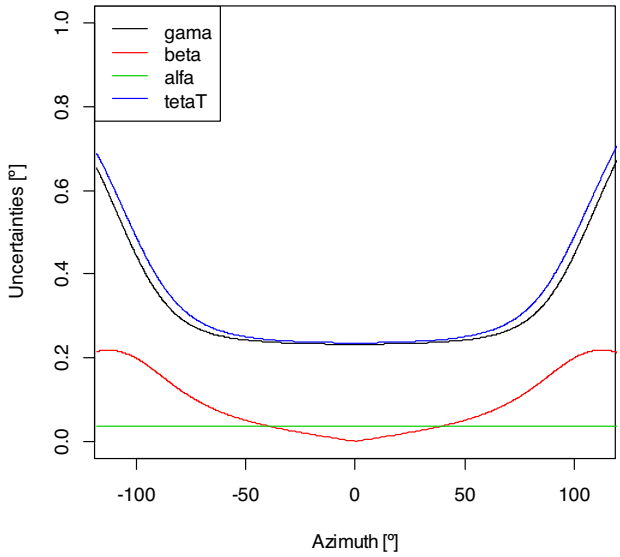

Figure 7: Transversal incidence angle uncertainty vs the solar azimuth

The u(θ_T) value is about 0.3° for azimuth angle γ_s between -90 and 90°, and up to 0.6° at the extreme azimuth

The uncertainty of the optical losses, $u(\Delta\eta_{track})$, according to Eq. 11 were calculated. Fig.8 shows the uncertainty $u(\Delta\eta_{track})$ ("optical losses" in black) calculated with its different uncertainty sources $u(\theta_T)$ $\delta\Delta\eta_{track}/\delta\theta_T$ (tetaT in red) and $u(K_b(\theta_T))$ $\delta\Delta\eta_{track}/\delta K_b(\theta_T)$ (Simulation IAM curve in green).

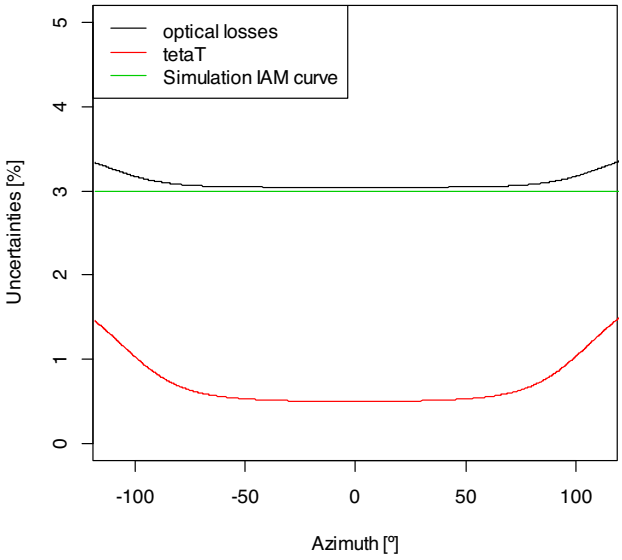

Figure 8: Optical losses uncertainty vs the solar azimuth

The mean optical error uncertainty was more that 3% but the main uncertainty source is the simulation IAM curve. The optical error uncertainty source due to incidence angle $u(\theta_T)$ $\delta\Delta\eta_{track}/\delta\theta_T$ is around 0.5%.

5. Conclusions

The optical and thermal characterisation of a medium temperature solar collector was performed based on ISO 9806 (2013) standard based on a two months monitoring data obtained from an installation in Malta. Unfortunately, the characterization was not correctly done due to a lack of variability in the inner temperature data and to some losses in the collector, which did not make it possible to maintain efficiency at the same temperature and to apply to ISO standard model to define it. The optical efficiency η_0 obtained was

30.9% ± 4.6% and the heat losses 0.317± 0.253 $W.m^{-2}K^{-1}$.

In a second step, the sensibility of the tracking is analyzed based on three rotation angles which defined the sun vector on collector plane. The tracking error was estimated as an uncertainty on the optical efficiency $u(\eta_0)$ of the collector. The maximum optical lost uncertainty due to incidence angle obtained was up to 0.5%, which could be one of the reasons of efficiency lower than expected, but not the main reason.

Future research would ensure that the optical and thermal characterization of the collector would be done with a more accurate testing bench in FBK Trento. Moreover, the tracking error would also be estimated by a home-made optical device which calculates the incidence angles on the collector planes using a webcam and image treatment.

6. Acknowledgements

The first author, Fabienne Sallaberry, would like to thank UPNA (Public University of Navarre) for financing her travel to Trento and the FBK (Fondazione Bruno Kessler) for financing her stay in its facilities.

The authors would also like to thank the participants of the project DIGESPO (project funded by European Committee FP-Energy-2009-1 call; www.digespo.eu) for authorization to use the testing data and photographs of the collector.

7. References

Alberti, F., Crema, L., Bozzoli, A., 2013. Design of a new medium-temperature Stirling engine for distributed cogeneration applications, Energy Procedia (ISSN:1876-6102).

Alberti, F., Crema, L., Bozzoli, A., 2012a. Heat Transfer Analysis for a Small-Size Direct-Flow Coaxial Concentrating Collector, ASME Journal of Solar Energy Engineering.

Alberti, F., Cozzini, M., Crema, L., Bartali, R., 2012b. Coating Candidates Comparison and a Two-Zone Coating Strategy for Parabolic Trough, 2012, Congress EuroSun 2012, Rijeka (Croatia).

Blanco-Muriel, M., Alarcón-Padilla, D.C., López-Moratalla, T., Lara-Coira, M., 2001. Computing the solar vector, Solar Energy. 70, 431-441.

Crema, L., Alberti, F., Wackelgard, E., Rivolta, B., Hesse, S., Luminari, L., Hislop, D., Restall, B., 2013. Novel system for distributed energy generation from a small scale concentrated solar power, Energy Procedia (ISSN:1876-6102).

ISO 9806, 2013. Solar Energy - Test method for solar collectors - Part 1: Thermal performance of glazed liquid heating collectors including pressure drop.

ISO/IEC, 2008. Uncertainty of measurement - Part 3: Guide to the expression of uncertainty in measurement (GUM), ISO/IEC Guide 98-3.

Marion W. F. and Dobos A. P. 2013. "Rotation Angle for the Optimum Tracking of One-Axis Trackers". Technical report. Technical report NREL/TP-6A20-58891.

Rabl, A., O'Gallagher, J., Winston, R., 1980. Design and test of non-evacuated solar collectors with compound parabolic concentrators, Solar Energy, 25, 335-351.

Pujol Nadal, R., Martínez Moll, V., 2012. Optical Analysis of the Fixed Mirror Solar Concentrator by Forward Ray-Tracing Procedure, Journal of Solar Energy Engineering, 134, 031009-031009.

Pujol-Nadal, R., Martínez-Moll, V., 2014. Parametric analysis of the curved slats fixed mirror solar concentrator for medium temperature applications. Energy Conversion Management 78, 676-83.

Sallaberry, F., Pujol Nadal, R., Martínez Moll, V., Torres, J-L., Optical and thermal characterization procedure of a variable geometry concentrator: a Standard approach, Renewable Energy 68 (2014) 842-852

Zaaiman, W., Taylor, N., 2011. Procedure for the determination of the accetance angle of CPV devices under natural solar illumination.